Unsteady Flow past Multiple Airfoils in Formation

Ravindra A Shirsath [1] and Rinku Mukherjee[2]

[1]*MS Scholar, Department of Applied Mechanics, Indian Institute of Technology, Madras, India 600036*

[2]*Assistant Professor, Department of Applied Mechanics, Indian Institute of Technology, Madras, India 600036*

Email: *aero.ravi22@gmail.com*

ABSTRACT

This paper presents the results of a numerical simulation of unsteady, incompressible and viscous flow past a single NACA0012 airfoil and two such airfoils in formation. The two airfoils in formation perform differently than when operating alone. The aerodynamic performance of the airfoils in formation and their effect on each other are therefore studied in detail. The formation is studied for different relative positions of the two airfoils and also by varying the angle of attack of the trailing airfoil. It is expected that such variations will affect the way in which the trailing edge vortices shed by the leading airfoil interact with the trailing airfoil. Consequently the performance of the trailing airfoil will be affected and will be different from the case if it were operating alone. The analysis is carried out using the the SST k-ω model of the commercial software package FLUENT 6.2. The Reynolds number for the study is 2.88×10^6 based on the free-stream velocity and the chord length of either of the airfoils. Both airfoils are of the same chord length. The results obtained as a part of this study include the unsteady coefficients of lift, drag and pitching moment as a function of the angle of attack of the trailing airfoil, i.e. $C_l(t)$-α, $C_d(t)$-α, $C_m(t)$-α. The results from the current study are compared with literature and found to be in very good agreement.

1. INTRODUCTION

The concept of formation flight is not new. It is however, more commonly attributed to large birds and in recent times has gained popularity in lieu of its applicability in various aerospace applications. Formation flight studies on real aircrafts have shown decrease in induced drag on the trailing aircrafts as well as longer range achievement, which translates into significant fuel savings, Bangash et al [1] and Vachon et al [2]. Fuel consumption is an important consideration and formation flight could provide some answers especially for longer range freight travel.

Creation of micro-UAVs which is motivated by insect flight has opened up yet another field for researchers to focus. Such vehicles are designed for very small payloads for remote-sensing operations where access is limited due to various hazards. Defence applications are ample as well and the use of multi-UAVs in formation for surveillance purposes will increase their longevity and endurance.

Computational implementation of these phenomena resulting in unsteady flight involves a numerical representation of the lifting surface as well as the wake behind it. In addition, when multiple lifting surfaces in tandem exhibit unsteady motion, which in other words is the case of unsteady formation flight, vortex-vortex as well as vortex-solid boundary interactions have to be taken into account.

Multiple lifting surfaces working in tandem have several applications and therefore researchers have always had interest and have undertaken studies where multiple lifting surfaces are interacting with each under different flight conditions. Some practical examples of lifting surfaces operating in tandem are that of the unsteady motion of rotorcrafts, aircrafts with multiple lifting surfaces like wing-canard and wing-tail configurations, multi-bladed vertical axis wind turbines, industrial mixers, turbine blades, food mixers, blenders, grinders etc.

Ahmed et al [3] numerically simulated the steady flow in a linear cascade of multiple airfoils using a control volume approach by solving the k-ε model of a 2D, incompressible N-S equations.

Fanjoy et al [4] studied the tandem-airfoil interactions in different regimes using computational methods. A two dimensional tandem airfoil geometry

comprising two NACA airfoils was tested at subsonic and sonic speeds. The results showed that, at positive angles of attack, the lift/drag ratio of the lead airfoil is increased while the trailing airfoil experiences less lift and drag, due to reduced local angle of attack.

Zannetti et al [5] analytically addressed the unsteady two dimensional rotational flow past doubly connected domains. Flow was modeled as a potential flow with point singularities, by concentrating the vorticity in point vortices. The dependence of the complex potential on time was defined according to Kelvin's theorem. Vortex shedding and time evolution of circulation past a two-element airfoil and past a two-bladed Darrieus turbine was studied as physical examples.

Hussain et al [6] did a two-dimensional analysis of tandem/staggered arranged airfoils of the canard and wing of an Eagle 150 aircraft using computational fluid dynamics and also conducted aerodynamic tests in an open-circuit wind tunnel. The wind tunnel experiments gave the optimum position for the wing and was validated by simulation. It was also observed in the simulation results that with the tandem position, the wake created by the leading airfoil disturbs the in-flow at the trailing airfoil.

Aziz et al [7], in a recent work undertook a 2D unsteady analysis of flow past two airfoils impulsively set into motion. A lumped vortex model is used to simulate the airfoils and the two individual wakes are simulated using discrete force-free vortices. A time-stepping method is used to predict the individual wake shapes. The effect of airfoil-airfoil and airfoil-wake interactions on the aerodynamic characteristics of each airfoil is studied. Numerical singularities due to airfoil and free wake vortices and due to interactions of free wake vortices with each other are accounted for to predict a smooth wake shape for each airfoil.

The objective of this study is to study such vortex-vortex and vortex-solid body interactions using CFD and use the results of such studies for analysis as well as preliminary information for design of formations.

2. NUMERICAL METHOD

2.1 Governing equations

In the present study, the fluid flow is modeled as 2D, incompressible, unsteady and viscous over a NACA0012 airfoil. The governing partial differential equation in the Reynolds averaged form for mass and momentum conservation are as follows.

$$\frac{\partial \bar{u}_i}{\partial x_i} = 0 \tag{1}$$

$$\frac{\partial \bar{u}_i}{\partial \tau} + \bar{u}_j \frac{\partial \bar{u}_i}{\partial x_j} = -\frac{\partial \bar{p}}{\partial x_i} + \frac{1}{Re}\frac{\partial^2 \bar{u}_i}{\partial x_j \partial x_j} + \frac{\partial \tau_{ij}^R}{\partial x_j} \tag{2}$$

In the above equation $\bar{u}_i$ refers to mean velocity either in the stream wise x direction or cross stream y direction. The velocities in x and y directions are normalized with respect to the free-stream inlet velocity U_∞. All geometric length scales are normalized using the chord length of either of the airfoils, c. The physical time is normalized with $\frac{c}{U_\infty}$ and pressure by ρU_∞^2, where ρ is the fluid density.

Due to the statistical averaging process, the Reynolds stress tensor τ_{ij}^R gets generated out of the convective non-linearity. In the present study, closure is achieved by introducing a shear stress transport (SST) k-ω turbulence model, where k is the turbulent kinetic energy and ω is the specific dissipation rate.

2.2 Geometry, mesh and boundary conditions

The domain used in the analysis for a single airfoil is shown in Fig. 1 and the domain used for the tandem airfoils is shown in Fig. 2.

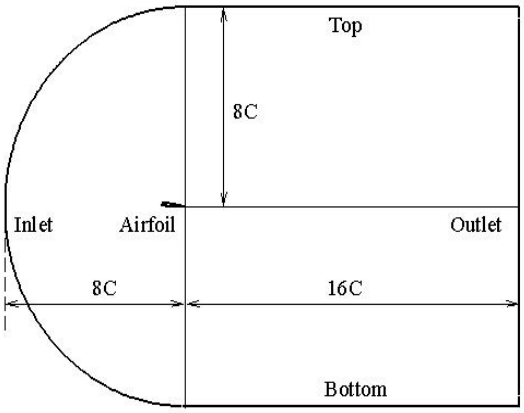

Fig 1. Domain for single airfoil.

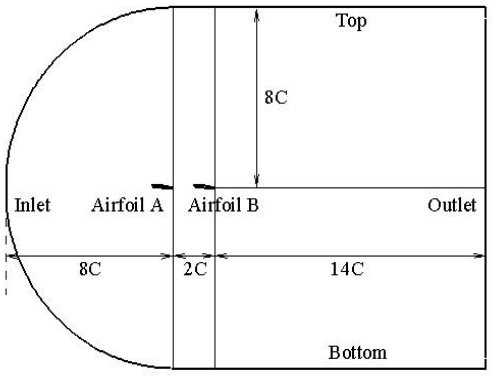

Fig 2. Domain for two airfoils in formation.

The domain for the single airfoil extends 8*c* upstream to 16*c* downstream and 8*c* to the upper and lower boundaries. The domain for the tandem airfoils is also of similar dimensions with respect to the leading airfoil. In addition, the trailing airfoil is placed 2*c* behind the leading airfoil.

The mesh used is dense in the vicinity of the airfoil(s) and a sample mesh is for the single airfoil is shown in Figs. 3 and 4.

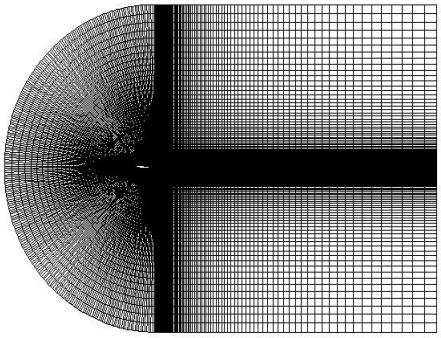

Fig 3. Mesh for single airfoil.

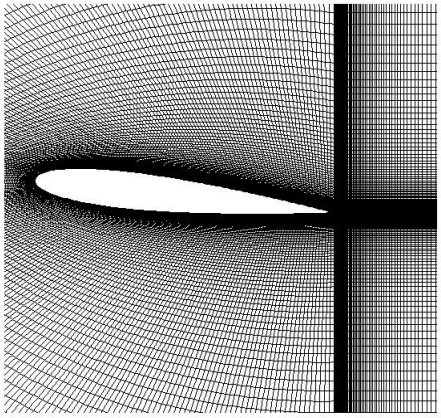

Fig 4. Mesh (zoomed) for single airfoil.

2.3 Testing conditions and analysis

At the inlet, the absolute magnitude of the components of the velocity of air are specified. In this case the velocity is parallel to the horizontal axis. The turbulence intensity is specified as 1% and the turbulent length scale is set to 0.0088. The upper and lower surfaces of an airfoil are set as walls. At the outlet, the pressure is set as atmospheric pressure. The lateral walls of the domain are set as symmetry. A time step of 0.001s is chosen and 60 sub iterations per time step are performed. The Re, calculated based on the free-stream velocity and airfoil chord length is 2.88×10^6. The results are obtained with the SST k-ω turbulence model with the y^+ value in the range of 30 to 60.

3. RESULTS

Results are presented for a single and a set of tandem airfoils. Validation is provided first and case studies from the current work follow.

3.1 Validation

Results from Gregory et. al. [8] are used for validation of the flow past a single NACA0012 airfoil. The variation of C_p over chord for $\alpha=0^\circ$ and $\alpha=6^\circ$ from Gregory and the current work are shown in Figs. 5 and 6 respectively.

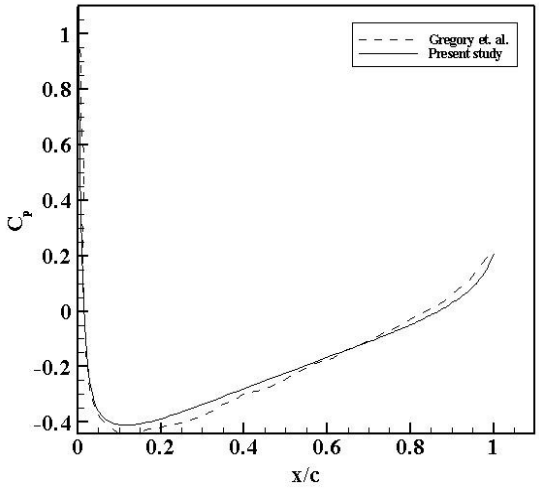

Fig 5. C_p over NACA0012 airfoil at $\alpha = 0^0$.

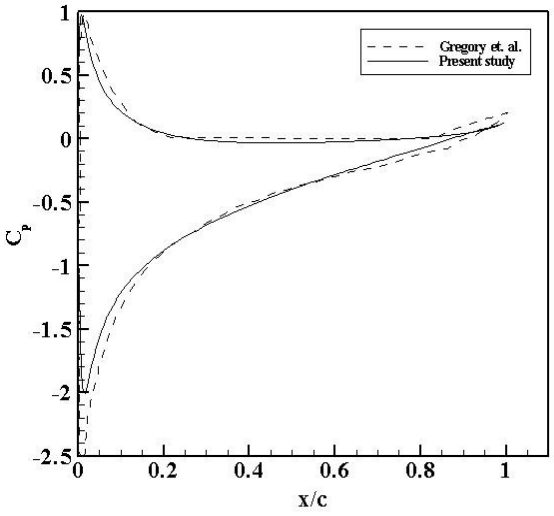

Fig 6. C_p over NACA 0012 airfoil at $\alpha = 6^0$.

3.2 Airfoils in formation

The $C_l(t)$ of the tandem airfoils for different physical distances between them are shown in Fig. 7-10. The angles of attack of both airfoils in all the cases mentioned above are 6^0.

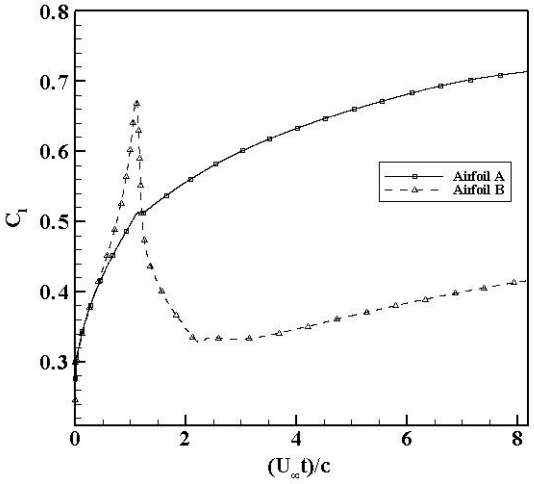

Fig 7. $C_l(t)$, airfoil B is 2c downstream of airfoil A

$$\alpha_A = \alpha_B = 6^0$$

It can be seen from Fig. 7, where the distance between the two airfoils is 2c, that there is a spike in the $C_l(t)$ of the trailing airfoil, B, around $\frac{U_\infty t}{c} = 1$. Similar spikes are also seen when the distance between the airfoils is increased to 3c and 4c in Figs 8 and 9 respectively but their occurance is delayed. The spike in Fig. 8 occurs around $\frac{U_\infty t}{c} = 2$ and in Fig. 9 occurs around $\frac{U_\infty t}{c} = 3$.

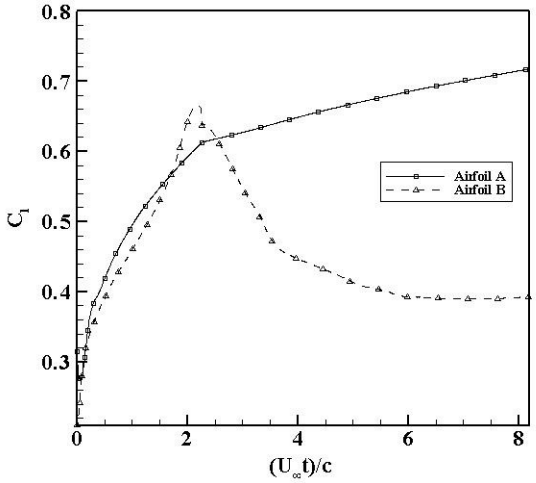

Fig 8. $C_l(t)$, airfoil B is 3c downstream of airfoil A

$$\alpha_A = \alpha_B = 6^0$$

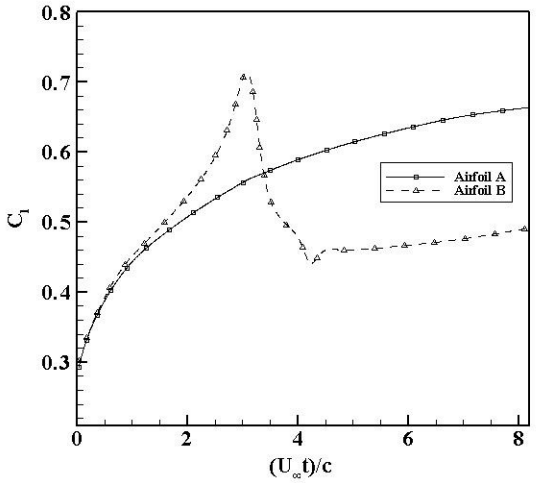

Fig 9. $C_l(t)$, airfoil B is 4c downstream of airfoil A

$$\alpha_A = \alpha_B = 6^0$$

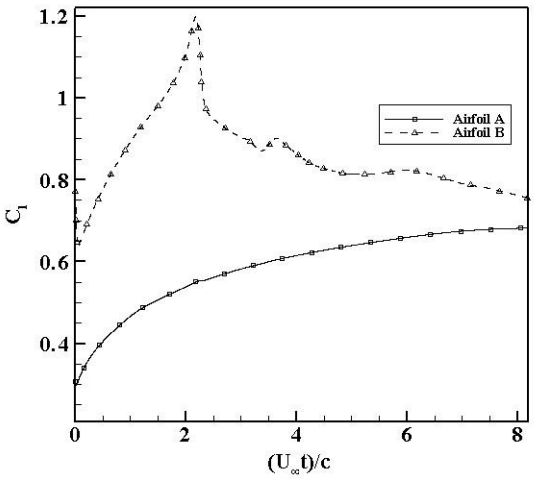

Fig 10. $C_l(t)$, airfoil B is 3*c* downstream of airfoil A $\alpha_A = 6^0, \alpha_B = 12^0$

In Fig. 10 the airfoils are at different angles of attack, airfoil B is at a higher angle of attack than airfoil A. The pattern of the $C_l(t)$ for airfoil B is similar to the cases shown in Figs. 7-9 but in this case it stays higher than that of airfoil A the entire time length considered. The peak occurs around $\frac{U_\infty t}{c} = 2$.

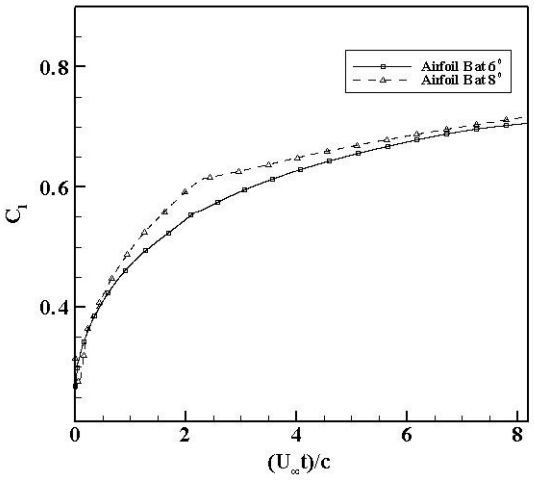

Fig 11. $C_l(t)$ of airfoil A when airfoil B is 3*c* downstream of airfoil A; $\alpha_A = 6^0$.

In Figs. 11 and 12, the effect of the two airfoils on each other is shown. Airfoil A is operating at $\alpha = 6°$ and the angle of attack of airfoil B is varied from $\alpha = 6°$ to $\alpha = 8°$.

In Fig 11, the effect of the trailing airfoil B on the leading airfoil A is shown.
It is seen that the change in angle of attack of the trailing airfoil affects the $C_l(t)$ of the leading airfoil.

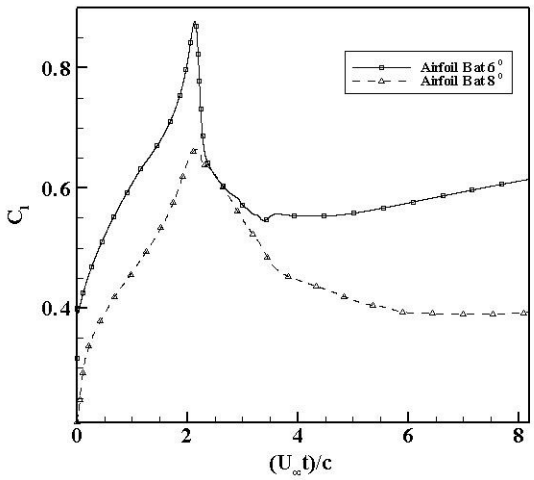

Fig 12. $C_l(t)$ of airfoil B when airfoil B is 3*c* downstream of airfoil A; $\alpha_A = 6^0$.

In fig 12, the $C_l(t)$ of airfoil B is shown. It is observed that the peak in both cases occurs at the same time instant but for the higher angle of attack of airfoil B, it is higher in magnitude as compared to the smaller angle of attack of airfoil B case.

3.3 Mesh dependency analysis

Mesh dependency test is conducted for the variation of C_l, C_d and C_p over an airfoil at *Re=2 x 10*^{6} and $\alpha = 6°$ with three different mesh sizes and is shown in Table 1 and Fig. 13 respectively.

Number of cells	Lift coefficient C_l	Drag coefficient C_d
12000	0.540868	0.026098
24000	0.542933	0.025716
36000	0.543795	0.025140

Table 1: Grid dependency Test

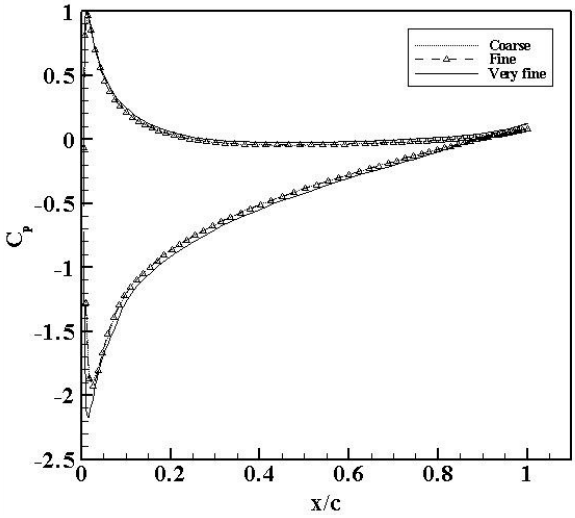

Fig 13. C_p over NACA 0012 airfoil at α=6° with three different mesh sizes.

Nomenclature

c	Chord length of an airfoil
k	Turbulent kinetic energy
ω	Specific dissipation rate
α	Angle of attack of an airfoil
C_p	Coefficient of pressure
C_l	Coefficient of lift
C_d	Coefficient of drag
Re	Reynolds number
U_∞	Free stream velocity
ρ	Free stream density

REFERENCES

[1] Z..A. Bangash, R.P. Sanchez and A. Ahmed. Aerodynamics of formation flight. *Journal of Aircrafl*, 43(4):907–912, 2006

[2] M. Vachon, R. Ray, K. Walsh and K. Ennix. F/A-18 aircraft performance benefits measured during the autonomous formation flight project. *AIAA,* 2002–4491, 2002

[3] N. Ahmed, B.S. Yilbas and M.O. Budair. Computational study into the flow field around a cascade of NACA 0012 airfoils. *Computer methods in Applied Mechanics and Engineering*, 167:17–32, 1998

[4] D. Fanjoy and D.J. Domey. A study of tandem airfoil interaction in different flight regimes. *AIAA,* 97-0515, 1997

[5] L. Zannetti, F. Gallizio and G.M. Ottino. Vortex motion in doubly connected domains. *Journal of Fluid Mechanics*, 612(11):143–152, 2008

[6] Z. Husain, M.J. Abdullah and T.C. Yap. Two-dimensional analysis of tandem/staggered airfoils using computational fluid dynamics. *International journal of Mechanical Engineering Education*, 33/3

[7] H. Aziz and R. Mukherjee. Unsteady aerodynamics of multiple airfoils in configuration. *AIAA Paper*-3523, 2011

[8] N. Gregory and C.L. O'Reilly. Low speed aerodynamic characteristics of NACA 0012 airfoil section , including the effects of upper surface roughness simulating hoar frost. *National physics laboratory*, Aero report, 1308, 1973

[9] FLUENT version 6.2 user manual 2005